

# Long-term multiwavelength periodicity on the light curves of Mrk 501: the case for an eclipsing supermassive binary black hole

Gustavo Magallanes-Guijón\* and S. Mendoza†

<sup>1</sup>*Instituto de Astronomía,  
Universidad Nacional Autónoma de México,  
AP 70-264, Distrito Federal 04510,  
México*

(Dated: October 31, 2022)

Using multifrequency observations, from radio to  $\gamma$ -rays of the Blazar Mrk 501, we constructed their corresponding light curves, and built its periodograms using RobPer and Lomb-Scargle algorithms. Long-term variability was also studied using the Power Density Spectrum, the Detrended Function Analysis using the software VARTOOLS. The result of these techniques showed an achromatic periodicity  $\lesssim 229$  d. This combined with the result of a pink colour noise in the spectra lead us to propose that the periodicity was produced by a secondary eclipsing supermassive binary black hole orbiting the primary one locked inside the central engine of Mrk 501. We built a relativistic eclipsing model of this phenomenon using Jacobi elliptical functions finding a periodic relativistic eclipse occurring every  $\sim 225$  d in all the studied wavebands.

## I. INTRODUCTION

Among Active Galactic Nuclei (AGN), Blazars are objects that emit variable non-thermal radiation throughout the electromagnetic (EM) spectrum (Padovani *et al.*, 2012) with their jets pointing at an angle no more than  $\sim 30^\circ$  from the observer's line of sight (Ulrich, Maraschi, and Urry, 1997). These extragalactic sources present total luminosities in the range  $10^{41} - 10^{47}$  ergs/s (see e.g. Blandford, Meier, and Readhead, 2019).

The light curve of a quasar in a certain frequency presents a natural variability due to real physical phenomena of the source and/or to observational errors. However, when the variability exceeds a factor  $\gtrsim 2$  from the mean observed value in a particular period of time, then it can in principle represent a physical phenomenon produced by the emitting source. In order to account for this, it is common to catalogue these quasi-periodic oscillations (QPOs) of Blazars in (a) intraday variability (IDV), corresponding to periods of over a day or less (Wagner and Witzel, 1995) –they are also called intra-night variability or micro-variability (Miller, Carini, and Goodrich, 1989), (b) short-term variability (STV) which corresponds to a variability over days to several weeks, and (c) long-term variability (LTV) that takes place on timescales of months to years (Gupta *et al.*, 2004).

There have been many physical proposals to explain variabilities in AGN, e.g. (a) A supermassive binary black hole companion (Lehto and Valtonen, 1996); (b) Accretion disc based events (Stella and Vietri, 1998); and (c) Jet geometry (Camenzind and Krockenberger, 1992; Mohan and Mangalam, 2015). Of particular relevance to the studies carried out in the present article is the case for postulating the existence of a secondary supermassive black hole orbiting about the primary one. The first proposal of this kind was made by Begelman, Blandford, and Rees (1980) in order to account for periodic or quasi-periodic oscillations.

To date, the best known example of a binary black hole system is that of the Blazar OJ 287, for which an extensive analysis of its optical light curve was used to infer this supermassive black hole binary system (Sillanpaa *et al.*, 1988). Its periodicity was discovered by analysing its historical optical light curve, which contains data from more than 100 years, showing repeated bursts at intervals of about 11.65 y. The best known model by Lehto and Valtonen (1996) consists of a primary black hole –the central engine, with mass  $\sim 17 \times 10^9 M_\odot$  surrounded by an accretion disc. A secondary black hole of mass  $\sim 10^8 M_\odot$  orbiting the primary one intersects on its orbit the accretion disc, causing tidal-induced mass fluxes from the accretion disc to the primary black hole.

An extensive survey to find periodic light curves in optical light was carried out by Graham *et al.* (2015). Of the 247000 studied light curves, it was found that the one corresponding to PG 1302-102 shows a periodicity of  $1884 \pm 88$  d.

\* Email address: gustavo.magallanes.guijon@ciencias.unam.mx

† Email address: sergio@astro.unam.mx

The authors assumed that this was due to the existence of a secondary black hole “eclipsing” the primary one and concluded that the system is separated by less than a parsec. More recently, Tavani *et al.* (2018) found 2.2 y QPOs in the  $\gamma$ -rays band of the Blazar PG 1553+113 and once again, proposed it as a supermassive black hole binary system.

A very interesting and quite well studied Blazar is Markarian 501 (Mrk 501). It is a BL Lac object with several periodicities reported in the literature: (1) A periodicity of 23 d was reported during a flare detected in X-rays and  $\gamma$ -rays (Rieger and Mannheim, 2000). (2) In the same frequencies, a periodicity of 72 d was found by Rödiger *et al.* (2009). (3) A periodicity of 630 d was discovered by Wang, Yin, and Xiang (2017) in X-rays. (4) Finally, Bhatta (2019) found a 332 d periodicity in the Fermi-LAT  $\gamma$ -rays light curve.

Mrk 501 has a redshift  $z = 0.034$  ( $\sim 456$  Mly  $\sim 140$  Mpc) with R.A. =  $16^{\text{h}} 53^{\text{m}} 52.2^{\text{s}}$ , Dec. =  $+39^{\circ} 45' 37''$ . It was discovered by Quinn *et al.* (1996) using the Whipple Imaging Atmospheric Cherenkov Telescope (IACT). It has been monitored since 1996 in various frequencies: radio (Richards *et al.*, 2011a), optical (Smith *et al.*, 2009), X-rays (Abdo *et al.*, 2011), and  $\gamma$ -rays (Dorner *et al.*, 2017).

In this article, we report a mean periodicity of  $224.07 \pm 0.22$  d in multi-frequency observations of Mrk 501. The dataset in radio was obtained from the Owens Valley Radio Observatory (OVRO)<sup>1</sup>, the optical one from The American Association of Variable Star Observers (AAVSO)<sup>2</sup>, the X-rays dataset is from The Neil Gehrels Swift Observatory (Swift)<sup>3</sup> and for  $\gamma$ -rays, the data was taken from the Fermi Gamma-Rays Space Telescope (FGST, also FGRST)<sup>4</sup>. These datasets and their corresponding processing (reduction) is explained in Section II. In Section III we describe different methods to find this multifrequency periodicity and in Section III.D we model this periodic behaviour assuming a supermassive binary black hole using Jacobi elliptical functions which have good representations of eclipses that produce occultations (as it occurs for binary stars or exoplanets eclipsing their central star) and magnifications (such as the ones that are produced by massive relativistic objects that bend light and magnify its intensity). Finally, in Section IV, we discuss our results.

## II. DATA AND LIGHT CURVES

The radio dataset from 2009 January 22 to 2020 June 27 was obtained from the OVRO database. OVRO consists of a 40 m telescope with a cryogenic receiver at a central 15 GHz frequency, a 3 GHz bandwidth and two symmetric off-axis beams. This observatory has been monitoring Blazars since 2008 (Richards *et al.*, 2011a) and one of its main targets is the search for QPOs and correlations between radio and  $\gamma$ -rays in Blazars (Abdo *et al.*, 2009; Ackermann *et al.*, 2011).

The optical AAVSO database is public and offers long-term datasets. It is an international organisation of variable star observers who participate in scientific discovery through variable star astronomy. It was founded in 1910 and their observations of variable stars are collected and archived for world-wide access in collaboration with amateur and professional astronomers. The light curve of Mrk 501 was built using the database from 1998 June 24 to 2021 September 12.

For the X-rays light curve, we used the Swift database from 2008 October 2 to 2021 October 8. This dataset contains energies in the range 0.3 – 10 keV. Swift has an X-Ray Telescope (XRT) with two important characteristics that makes it important for observations: low background and a constant point spread function across the field of view (Moretti *et al.*, 2005).

The public database GLAST of  $\gamma$ -rays has fluxes in the range 100 MeV – 300 GeV. For Mrk 501, it covers a time interval from 2008 August 04 up to 2020 March 13.

The data from the Swift and GLAST observatories were reduced by processing the files corresponding to both the photons and the position and the orientation of the satellite on Flexible Image Transport System format files (FITS) with the HEASoft<sup>5</sup> and Fermitools<sup>6</sup> software. In both cases, it is necessary to know the relevant parameters of the object in question, such as: right ascension, declination, energy interval, and starting and ending time of the data processing (see e.g. Magallanes-Guijón, 2020). The satellite information is reviewed to make various time and position corrections and with this the analysis of the maximum likelihood estimation is carried out where the FITS files will be used (see e.g. Cabrera *et al.*, 2013). Finally, a table is built that contains the light curve information, i.e. a file that contains discrete data of time, luminosity and its uncertainty. The time data is so precise that its associated with a zero uncertainty.

<sup>1</sup> <https://sites.astro.caltech.edu/ovroblazars/>

<sup>2</sup> <https://www.aavso.org/>

<sup>3</sup> <https://swift.gsfc.nasa.gov/>

<sup>4</sup> <https://fermi.gsfc.nasa.gov/>

<sup>5</sup> <https://heasarc.gsfc.nasa.gov/docs/software/lheasoft/>

<sup>6</sup> <https://fermi.gsfc.nasa.gov/ssc/data/analysis/software/>

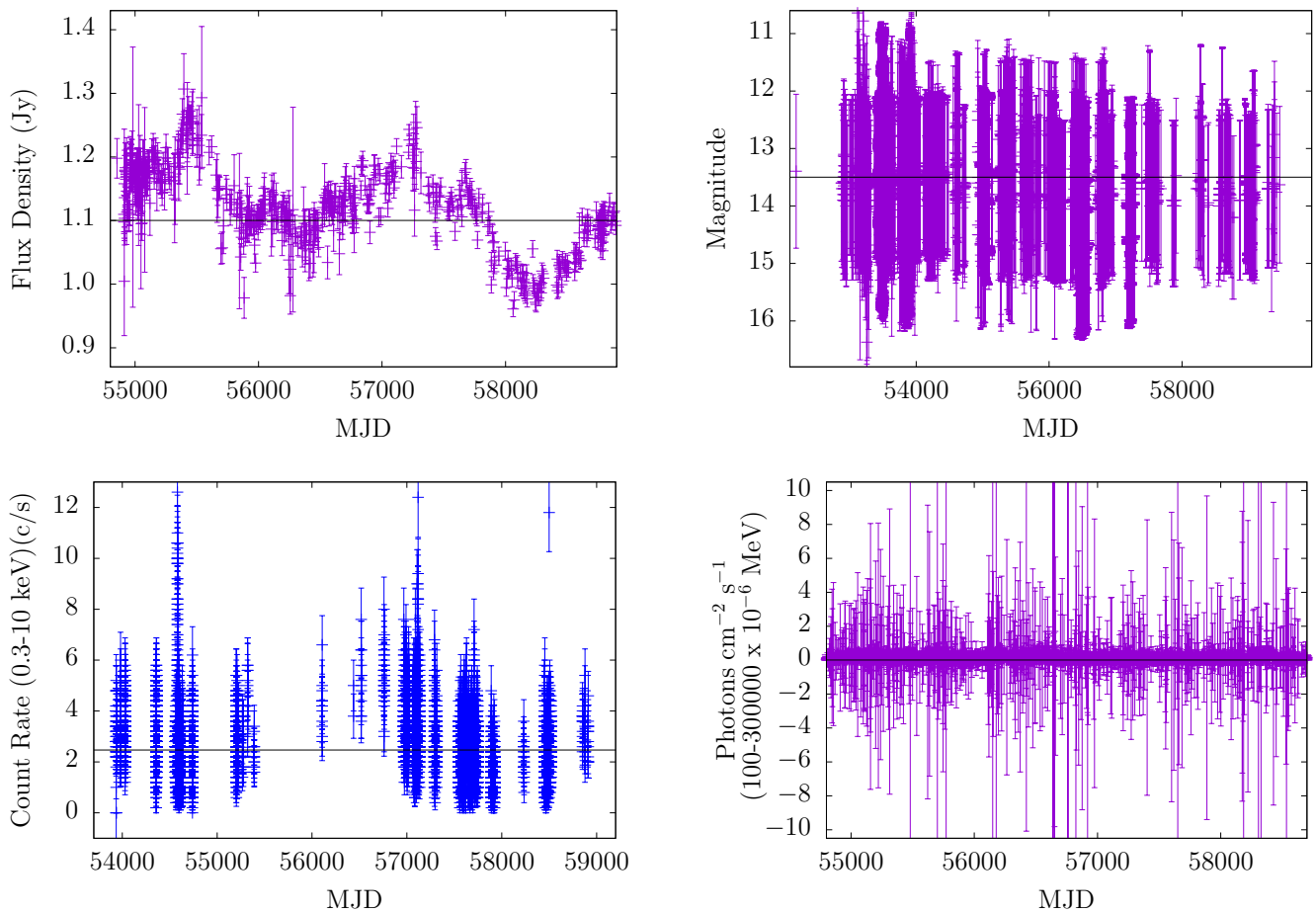


FIG. 1 Multifrequency light curves of the Blazar Mrk 501. From left to right and top to bottom, the panels represent radio, optical, X and  $\gamma$ -rays light curves as described in the text. The horizontal solid lines mark the mean value of the corresponding flux.

Band	Records	Interim (y, m, d)	Total (d)
Radio	615	11, 5, 5	4174
Optical	11, 849	23, 2, 17	8441
X-rays	28, 000	12, 7, 9	4607
$\gamma$ -rays	4, 199	11, 7, 9	4239

TABLE I The table shows each electromagnetic band studied for Mrk 501: the number of records, the interim in years, months, and days (y, m, d), and the total days for which at least a measurement is obtained (d).

The multifrequency light curves, resulting from processing the available data described above is presented in Figure 1. Table I shows the processed data in a synthesized way for all the electromagnetic frequencies studied for Mrk 501.

### III. METHODS

#### A. Periodograms and Window Functions

With the data processed, the search for periodicities was carried out. For this, the *R-package RobPer* was useful to analyse the associated periodograms on scales of time of several years. The RobPer package was built for the analysis

Band	RobPer (d)	L-S (d)	Mean (d)
Radio	228	228.06	228.03
Optical	228	225.54	226.77
X-rays	223	223.40	223.20
$\gamma$ -rays	237	240.80	238.90

TABLE II The table shows the time in days (d) for the peaks and their mean values of the RobPer and Lomb-Scargle algorithms in each electromagnetic band studied for Mrk 501.

of time series in astrophysics, in which there is the possibility of having data that is not necessarily equidistant in time (Thieler, Rathjens, and Fried, 2014). It is based on robustly fitting periodic functions of the time-series (light curves) in question and calculates periodograms with irregular (non-equidistant) observations on the time scale.

To support the RobPer periodogram analysis, a Lomb-Scargle (L-S) periodogram was also used. This algorithm was proposed by Lomb (1976) and Scargle (1982) and to date is the most used method for detecting periodicities in unevenly-sampled light curves. The L-S technique is based in Fourier Methods, Phase-folding Methods, Least Squares Methods and Bayesian Approaches (VanderPlas, 2018).

To avoid false positives in the detected periods with the RobPer and L-S routines, we built a windowing program following the work of Dawson and Fabrycky (2010) and apply it to all the electromagnetic bands studied. This window function  $W(\nu)$ , for a fixed frequency,  $\nu$  is given by:

$$W(\nu) = \frac{1}{N} \sum_{r=1}^N e^{-2\pi i \nu t_r}, \quad (1)$$

where  $N$  represents the total number of points in the dataset and  $t_r$  is the observation time of the  $r$ -th data. Under this method, false positives are ruled out by direct comparison of a  $W(\nu)$  vs  $\nu$  diagram and the periodograms obtained with RobPer and L-S. In this way, if there is a false positive periodicity in the data collection (such as e.g. an annual period of time due to vacation days in which no observations were taken) it will be presented as a peak in the window function (WF). The peaks that result as true positives in a periodogram are thus compared with their respective WF troughs in all the electromagnetic bands analysed. Figure 2 shows the periodograms obtained with RobPer and L-S with the corresponding time WF. The true mean peak in each periodogram is shown with a vertical dotted line. These mean periodicities are reinforced by the fact that the true mean peaks do not coincide with any peak in the WF.

one can be confident of their positivity.

## B. VARTOOLS

VARTOOLS<sup>7</sup> is an open-source command-line utility for analysing light curves developed by Hartman and Bakos (2016). It is written in the C programming language and provides a set of tools for processing, manipulating, and studying light curves. The routines implemented in VARTOOLS for studying Mrk 501 were the L-S periodogram, the Box-Least Squares (BLS), the Analysis of Variance (AoV), and the Discrete Fourier Transform (DFT).

AoV is a VARTOOLS routine for detection of sharp periodic signals based on the code developed by Devor (2005). This method consists on folding and binning data with a trial period. It has also been used by Schwarzenberg-Czerny (1989) for identifying and studying eclipsing binaries within large data sets of light curves.

The AoV-h VARTOOLS routine consists on the analysis of the variance using a multi-harmonic model. This method uses periodic orthogonal polynomials to fit the observations and the analysis of the statistical variance to evaluate the quality of the fit (Schwarzenberg-Czerny, 1996).

The plots of the AoV and AoV-h of Mrk 501 are shown in Figure 3, which result in an average periodicity of 231.78 d for the AoV and and 228.215 d for the AoV-h.

---

<sup>7</sup> The VARTOOLS free GNU General Public License software is available at: <https://www.astro.princeton.edu/~jhartman/vartools.html>

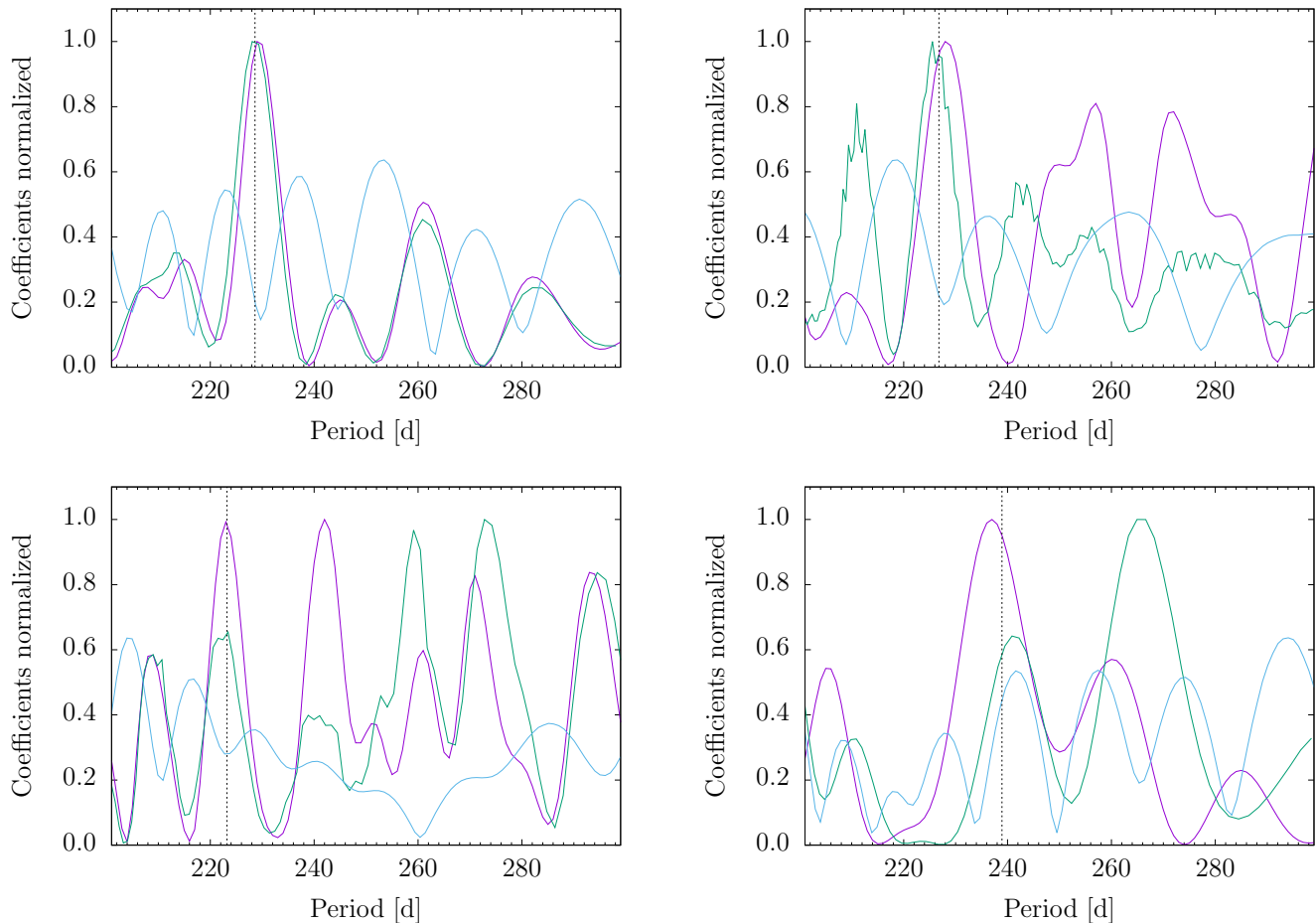


FIG. 2 RobPer (magenta) and L-S (green) periodograms together with their corresponding window function (blue) for radio, optical, X and  $\gamma$ -rays observations of Mrk 501 are shown from left to right, top to bottom panels. The black dotted vertical line shows the mean periodicity between the RobPer and L-S peaks which are common in all frequencies (Radio: 228.03 d, Optical: 226.77 d, X-rays: 223.20 d and  $\gamma$ -rays: 238.90 d). Table II shows the periods obtained for the periodograms presented on the Figure. The fact that these mean periodicities do not coincide with peaks in the window function reinforces their true periodicity character.

The VARTOOLS BLS routine is commonly used in studies of stellar photometric time series in the search for periodic transits of exoplanets (Kovacs, Zucker, and Mazeh, 2002). Using this routine for Mrk 501 we found a mean periodicity in all frequencies of 232.121 d -see Figure 4.

The VARTOOLS Discrete Fourier Transform (DFT) algorithm calculates the power spectrum of the time series (Roberts, Lehar, and Dreher, 1987). The routine to compute the DFT was developed by Kurtz (1985). A value periodicity of 229.959 d was obtained when DFT routine was applied to Mrk 501 in all frequencies -see Figure 4. Table III summarises the the periodicity results of VARTOOLS applied to Mrk 501.

### C. Power Spectrum Density, Detrended Fluctuation Analysis, and the colours of noise.

The study of time series -or light curves  $f(t)$  in the study of this article, with a sample length  $n$ , can be analysed using the Fourier transform  $P(\nu)$  given by (see e.g. Aschwanden, 2011):

$$P(\nu) = \frac{1}{n} \sum_{t=0}^{n-1} f(t) e^{-\frac{2\pi i \nu t}{n}}. \quad (2)$$

With this transform, it is possible to obtain specific periodic pulses in the light curve, even with excessive noise (see

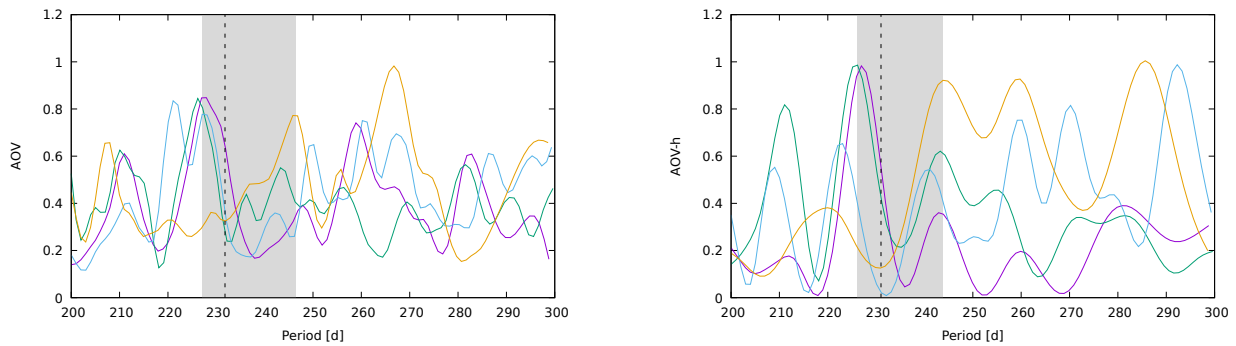


FIG. 3 The figure shows the Analysis of Variance (AoV) for Mrk 501 using VARTOOLS. The left panel is the AoV for all frequencies: radio in magenta with a periodicity of 227.2 d, optical in blue with a periodicity of 226.73 d, X-rays in green have a periodicity of 227.1 d and  $\gamma$ -rays in yellow with a periodicity of 246.1 d. The mean value of 231.78 d is represented with a dashed vertical line. The grey vertical band zone represents the statistical range of these mean values. The right panel uses the same colouring scheme as the left one but for the harmonic Analysis of Variance (AoV-h) of the VARTOOLS software. The periodicity of radio, optical, X-rays and  $\gamma$  rays are given by: 228.06 d, 227.4 d, 223.4 d and 234d respectively, yielding an average value of 228.215 d shown with the vertical dashed line. The vertical values on both panels were normalised to the maximum.

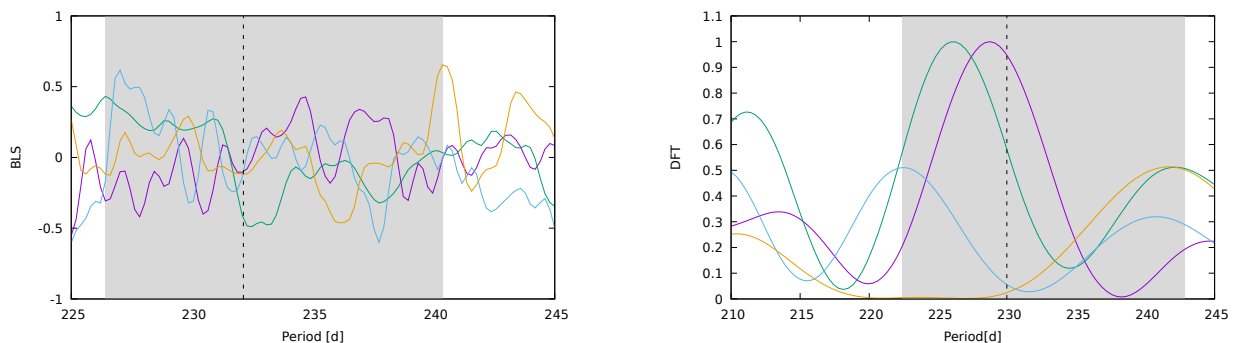


FIG. 4 The left panel shows the B-L Square algorithm of VARTOOLS used in all wave bands using the same colouring scheme of Figure 3, with the following periodicities in radio, optical, X-rays and  $\gamma$ -rays: 234.697 d, 226.414 d, 227.02 d, 240.354 d, with a mean value of 232.121 d represented by a dashed horizontal line. The right panel with the same colouring scheme uses the DFT VARTOOLS algorithm with resulting periodicities of: 228.737 d, 225.909 d, 222.374 d and 242.818 d with and an average value of 229.959 d. The vertical values on both panels were normalised to the maximum.

e.g. Press, 1978). If there are multiple periodic fluctuations present in the light curve, then the Power Spectral Density (PSD) will reveal each one with a peak in the power spectrum at the particular periodicity or frequency.

The PSD function approaches a power law at a particular frequency  $\nu$  given by:

$$P(\nu) = \nu^{-\alpha}, \quad (3)$$

for a fixed exponent  $\alpha$ . The spectral noise of the signal can be represented by its colour of noise (Press, 1978) depending on the value of  $\alpha$  as: white, pink, Brownian and black according to the values of Table IV.

A given colour of noise has statistical and correlation characteristics. When white noise predominates in the signal it means that there is no temporal correlation in a specific time series and the case of Brownian noise is obtained when a temporal correlation on the signal is significant (Schroeder and Wiesenfeld, 1991). Pink noise corresponds to the statistical case of phase change, in which there is a transition from a random process to a predictive one (May, 1976). The colours of noise analysis has been performed in the literature for time series of solar bursts, magnetospheric physics, binary black holes and other astrophysical phenomena (Aschwanden, 2010).

To support the PSD results, a Detrended Fluctuation Analysis (DFA) method (Peng *et al.*, 1994) on the time series can be computed for determining the statistical self-affinity in each frequency. DFA is useful also in the analysis of time series that appear to show long-memory processes. It is useful in the study of the chaos theory, stochastic processes, and time series analysis. The fluctuation  $F(n)$  is calculated for different window sizes  $n$  as:

Band	AoV (d)	AoV-h (d)	BLS (d)	DFT (d)
Radio	227.20	228.06	234.697	228.737
Optical	226.73	227.40	226.414	225.909
X-rays	227.10	223.40	227.020	222.374
$\gamma$ -rays	246.10	234.00	240.354	242.818
Averages	231.78	228.21	232.121	229.959

TABLE III The table shows the mean periodicity value of the AoV, AoV-h, BLS and DFT obtained with VARTOOLS for Mrk 501.

PSD exponent	Colours of noise
$0.0 \lesssim \alpha \lesssim 0.5$	white
$0.5 \lesssim \alpha \lesssim 1.5$	pink
$1.5 \lesssim \alpha \lesssim 2.5$	Brownian
$2.5 \lesssim \alpha \lesssim 0.5$	black

TABLE IV The table shows the intervals of the Power Spectrum Density (PSD) exponent  $\alpha$  of equation (3) and its associated colour of noise.

$$F(n) = \sqrt{\frac{1}{N} \sum_{t=1}^N (X_t - Y_t)^2}, \quad (4)$$

where  $N$  is time series length,  $X_t$  is the cumulative sum or profile of the time series and  $Y_t$  is the resulting piecewise sequence of straight-line fits (see e.g. Bryce and Sprague, 2012). The resulting  $\log F(n)$  vs.  $\log n$  measures the statistical self-affinity of the time series, expressed through a fixed  $\beta$  exponent from the following relation:

$$F(n) \propto n^\beta. \quad (5)$$

Table V shows that the application of a PSD and a DFA to the multi-frequency light curves of Mrk 501 results in a pink noise. For completeness, Figure 5 shows the PSD plots in all studied wavelengths.

#### D. Data fitting via a Jacobi elliptical function

The achromatic periodicity, from radio to  $\gamma$ -rays, of  $\lesssim 229$  d detected in the previous sections combined with the pink noise colour implies that a correlated phenomenon is producing it. The simplest way in which such a phenomenon may occur is with an eclipse as shown in Figure 6, since an orbiting massive object covering partially the radiation from the central parts of Mrk 501 will do so in a periodic way. In what follows we will denote the central supermassive

Band	$\alpha$	$\beta$
Radio	$1.24 \pm 0.02$	$1.287 \pm 0.0035$
Optical	$1.16 \pm 0.03$	$0.869 \pm 0.0045$
X-rays	$0.61 \pm 0.005$	$1.019 \pm 0.0045$
$\gamma$ -rays	$0.87 \pm 0.035$	$0.853 \pm 0.0015$

TABLE V The Table shows the obtained values for the exponents  $\alpha$  and  $\beta$  resulting from the PSD and DFA colour of noise analysis to the multi-frequency observations of Mrk 501. In all cases, the resulting colour of noise is pink according to the classification presented on Table IV, which implies that the light curves present temporal correlations with random fluctuations.

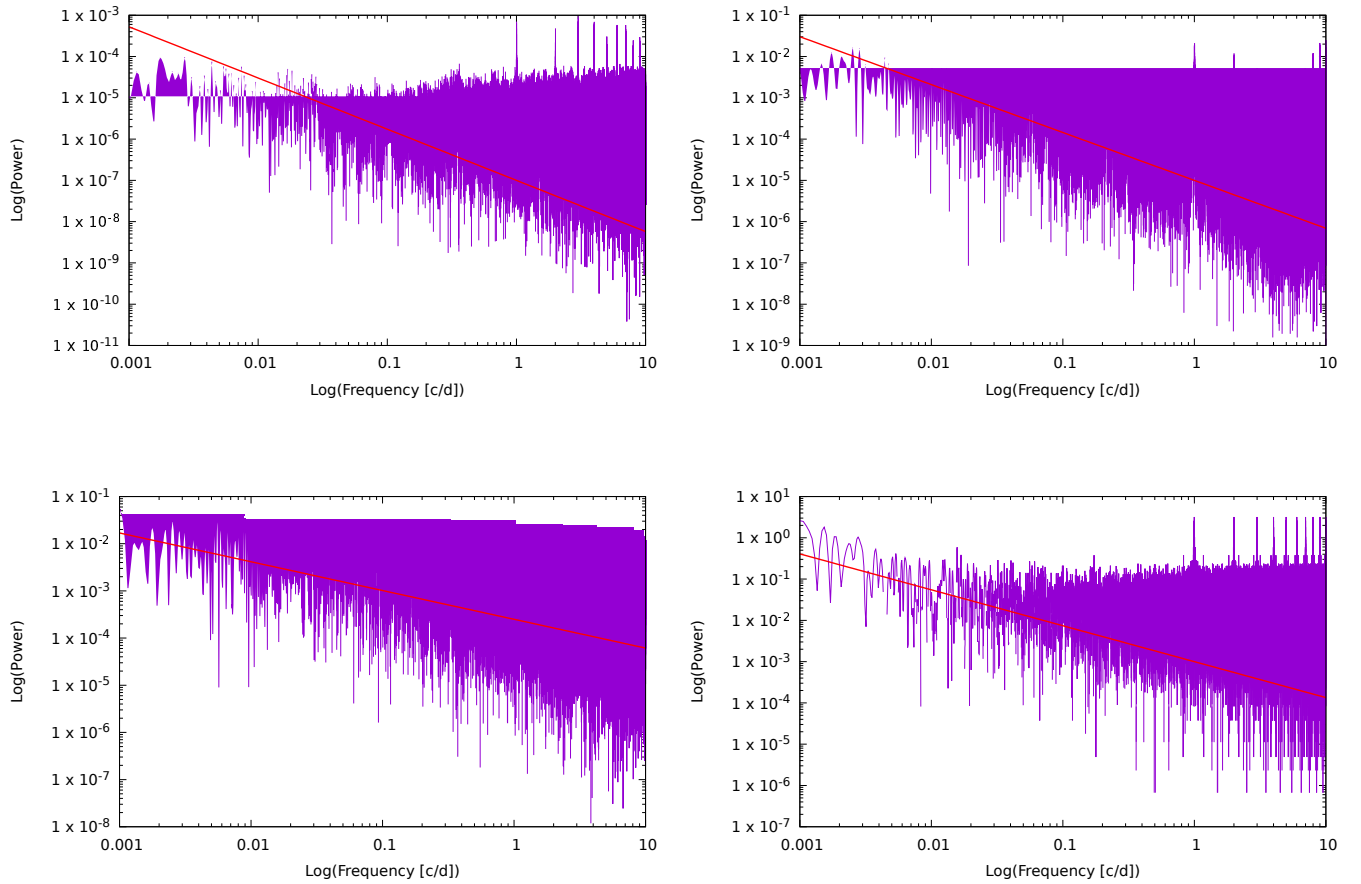


FIG. 5 From left to right and top to bottom, the panels on the Figure correspond to radio, optical, X-rays and  $\gamma$ -rays Power Spectrum Density (PSD) of the Blazar Mrk 501. In all cases, the colour of noise of the signal is pink according to the results of Table V.

black hole as the primary black hole and the eclipsing massive object as the secondary object. When light is obscured by a non-relativistic massive object it gets dimmed, as it happens in a standard eclipse of say, an eclipse produced by an exoplanet when it passes through the central star of its planetary system (Deeg and Belmonte, 2018). However, light is magnified if a relativistic object passes through light beams produced by a primary source of light (see e.g. Narayan and Bartelmann, 1996, and references therein). The following eclipse function  $e(t)$  serves as a good empirical way to model an eclipse:

$$e(t) = \pm \left\{ \Theta(t) - \Theta(t - \pi) \right\} \text{sn}^2 \left( \frac{2K(m)t}{\pi} \right) \quad (6)$$

where  $\Theta$  represents the Heaviside step function, sn is the elliptic sine, or sinus amplitudinis Jacobi function with module  $m$ , such that  $0 \leq m \leq 1$ , and  $K(m)$  is the complete elliptic integral of the first kind given by (see e.g. Abramowitz and Stegun, 1964):

$$K(m) = \int_0^{\pi/2} \frac{d\zeta}{\sqrt{1 - m \sin^2 \zeta}}. \quad (7)$$

The  $\pm$  sign on the right-hand side of equation (6) represents a standard non-relativistic eclipse, i.e. an eclipse that diminishes the amount of received radiation, for the minus sign and a magnification relativistic eclipse for the plus



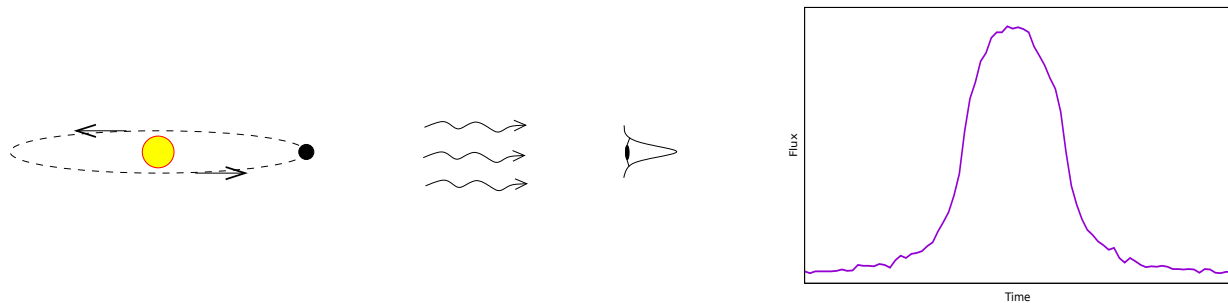


FIG. 6 The illustration shows an orbiting black hole about a central spherical source of light, that eclipses the radiation detected by an observer. For simplicity and in order to amplify the magnification effect detected by the observer, the example shown in the figure has the line of sight of the observer within the plane of the orbit. The right plot shows the radiation flux detected by the observer. It consists of a numerical simulation of a Schwarzschild black hole orbiting a fixed spherical source of light. Over an orbital period, the passage of the black hole through the line of sight of the observer magnifies the flux detected. The plotted flux and time are normalised to numerical units for a spherical source of radius five emitting isotropic radiation, a Schwarzschild radius of the black hole of one and for an orbit of radius thirty. The ray-tracing technique used for this simulation was performed using a squared screen normal to the line of sight at a distance of one thousand. A movie of this numerical simulation can be found at [https://archive.org/details/blackhole\\_magnification](https://archive.org/details/blackhole_magnification) and was done using a GNU General Public License (GPL) code named *aztekas-shadows* which is under development and will eventually be available at <https://aztekas.org>, Copyright ©2020 Gustavo Magallanes-Guijón, Sergio Mendoza & Milton Jair Santibañez-Armenta.

Band	$A$	$m$	$t_e$ days	$t_q$ days	$n$	$p$ days	$\langle f \rangle$	$A/\langle f \rangle$
Radio	$0.09758 \pm 0.00009$	$0.8577 \pm 0.0008$	$88.33 \pm 0.08$	$130.20 \pm 0.13$	$16.43 \pm 0.01$	$218.536351 \pm 0.21$	$1.1188 \pm 0.0222$	$0.08721 \pm 0.0001$
Optical	$1.18349 \pm 0.0018$	$0.1401 \pm 0.0001$	$89.76 \pm 0.08$	$133.18 \pm 0.13$	$35.03 \pm 0.03$	$222.947563 \pm 0.22$	$13.4850 \pm 1.3486$	$0.08776 \pm 0.0002$
X-rays	$0.99804 \pm 0.0009$	$0.8255 \pm 0.0008$	$89.37 \pm 0.08$	$137.05 \pm 0.13$	$19.96 \pm 0.01$	$226.434882 \pm 0.22$	$2.4648 \pm 0.6886$	$0.40491 \pm 0.0007$
$\gamma$ -rays	$0.99999 \pm 0.0009$	$0.2067 \pm 0.0002$	$86.25 \pm 0.08$	$142.10 \pm 0.14$	$17.69 \pm 0.01$	$228.365120 \pm 0.22$	$0.1368 \pm 0.4893$	$7.30986 \pm 0.0119$

TABLE VI The table shows the best fit of the eclipse model using a Montecarlo method for the multiwavelength data of Mrk 501. Columns represent electromagnetic wavebands, eclipse amplitude  $A$ , elliptic Jacobi function module  $m$  duration time of the eclipse  $t_e$ , interval of time where the eclipse is not occurring, i.e. quiescent time  $t_q$ , number of times  $n$  the eclipse occurred, total periodicity  $p := t_e + t_q$ , mean value of the flux  $\langle f \rangle$ , and the dimensionless brightness magnification produced by the eclipse  $A/\langle f \rangle$ .

sign. In the limit when the module  $m \rightarrow 1$ , a single squared pulse is obtained and when  $m \rightarrow 0$ , a sinusoidal curved profile is obtained.

To model the obtained periodicity on the light curves of Mrk 501 shown in the previous sections we built a C program capable of dealing with the expectations of an eclipse fingerprint produced on a long-term light curve based on a modification of equation (6). The program has as free parameters, the amplitude  $A$  of the eclipse, the duration time  $t_e$  of the eclipse, the quiescent duration time  $t_q$  when the eclipse is not occurring and the number of occurrences of the eclipse  $n$ . We have chosen the statistical average  $\langle f \rangle$  as the zero or quiescent flux of the light curve. A set of artificial examples of these eclipses are presented in Figure 7.

The data fitting for Mrk 501 was performed using a Montecarlo method based on the program mentioned in the previous paragraph. Random seeds were used for the unknown parameters of the program using  $10^6$  attempts for each light curve for a Gaussian noise. Table VI shows the results of the fit for each waveband.

#### IV. DISCUSSION

Different analysis on the long-term multiwavelength (from radio to  $\gamma$ -rays) light curves of Mrk 501 show a common achromatic periodicity of  $\lesssim 229$  d. The Montecarlo fitting technique assuming a relativistic eclipse as the cause for this periodicity shows a periodicity of  $\sim 224$  d. The eclipse is produced by a secondary supermassive black hole orbiting about the primary supermassive black hole, i.e. about the central engine, of Mrk 501. The reasoning for this conclusion is summarised in the following paragraphs.

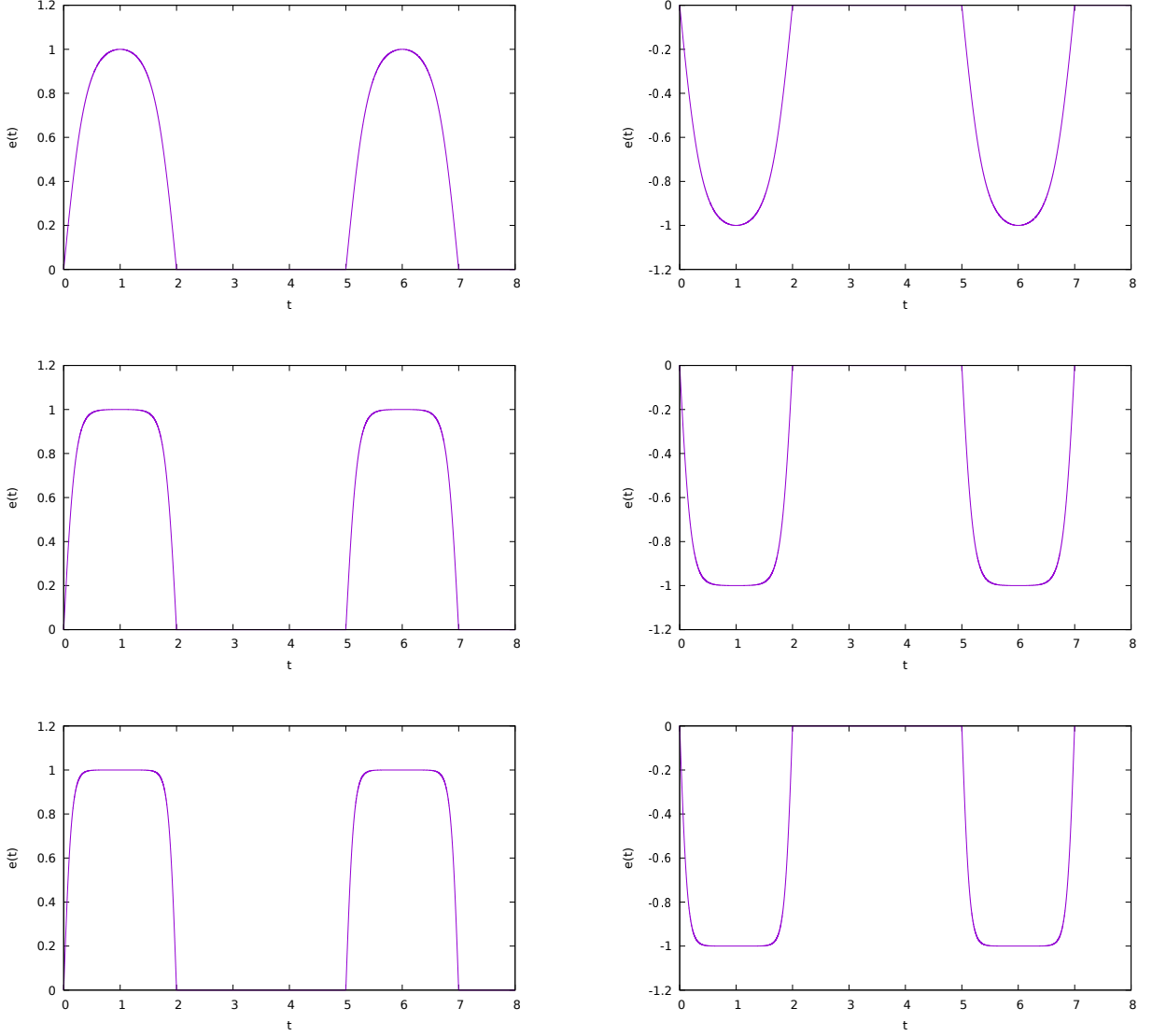


FIG. 7 The figure shows plots of an artificial eclipse that occurs two times. The software that produced them is described in section III.D and is Copyright ©2022 Gustavo Magallanes-Guijón & Sergio Mendoza. From top to bottom, different values of the Jacobi elliptic function  $m = 0.9, 0.999, 0.99999$  were chosen and for all plots the duration time of the eclipse  $t_e = 2$  for a quiescent time  $t_q = 3$  and an amplitude  $A = 1$ . The left column shows relativistic eclipses that produce magnification, which correspond to a plus sign in the simplified equation (6), and the right column represents a standard non-relativistic eclipse showing diminishing of the radiation represented by a minus sign in the same equation.

The periodicities found with the RobPer and L-S algorithms described in Section III.A are all consistent in all frequencies of Mrk 501 with average values in radio, optical, X-rays and  $\gamma$ -rays respectively given by: 228.03, 226.77, 223.20 and 238.90 days according to the results of Table II. The mean value for these periodicities is 229.225 d.

With the use of the VARTOOLS software described in Section III.B, we found that for the AoV, AoV-h, BLS, and DFT routines, the periodicity value lies in the intervals: 226.73–246.1, 223.4–234, 226.414–240.354, 222.374–242.818 days respectively, according to the results presented in Figures 3 and 4.

The fact that the colour of the signal noise in the light-curves of Mrk 501 presented in section III.C is pink, means that for each particular waveband there is a robust oscillation (Brownian noise colour) with a periodicity accompanied by a random signal (white noise colour).

Due to the achromatic nature of the found periodicity of  $\lesssim 229$  d, we modelled this periodicity as a relativistic eclipse caused by an orbiting supermassive black hole about the central engine of Mrk 501. The results of Table VI show that this model is quite coherent in the fitting of the long-term multi-frequency light curves. The only small

inconsistency found is with the dimensionless brightness magnification  $A/\langle f \rangle$  presented in X-rays and more prominent in  $\gamma$ -rays. This is most probably due to the large reported errors in  $\gamma$ -rays and the large gaps that appear in the X-rays light curve. Figure 8 shows a time-folding of the multi-frequency light curves with the corresponding eclipse function using the results of Table VI. The shaded region represents the time duration  $t_e$  of the eclipse.

Using the results of Table VI and Kepler's third law for a circular orbit given by:

$$v = \frac{r_{\text{orbit}}}{p} = \sqrt{\frac{GM_{\text{prim}}}{r_{\text{orbit}}}}, \quad (8)$$

where  $v$  is the velocity of the orbiting test mass (secondary black hole),  $r_{\text{orbit}}$  and  $p$  are the radius and period of the orbit,  $M_{\text{prim}}$  the mass of the central supermassive black hole and  $G$  represents Newton's constant of gravitation, it follows that:

- The mass of the central (primary) black hole in Mrk 501 is  $M_{\text{prim}} \sim 10^9 M_{\odot}$  which means that its gravitational radius  $r_{g\text{-prim}} \sim 20$  au.
- The radius of the orbit of the eclipsing (secondary) binary black hole is  $\sim 200$  au  $\sim 10 r_{g\text{-prim}}$ .
- The orbital period of the eclipsing binary black hole is  $\sim 224$  d.
- The orbital velocity of the eclipsing binary black hole is  $\sim 0.3\%$  of the speed of light, i.e.  $\sim 3 \times 10^6$  km/h.
- The brightness magnification of the radiation produced by an eclipse due to the secondary black hole is  $\gtrsim 10\%$ .

## V. ACKNOWLEDGEMENTS

This work was supported by a PAPIIT DGAPA-UNAM grant IN110522. GMG and SM acknowledge support from CONACyT (378460,26344). The authors thank discussions and comments from Erika Benitez while preparing this work. We are also grateful to Milton Santibañez-Armenta for the discussions and programming help for the black hole eclipsing video that supports the results of this work. We thank the OVRO 40-m monitoring program (Richards *et al.*, 2011b) for the radio database. The public OVRO database is supported by private funding from the California Institute of Technology and the Max Planck Institute for Radio Astronomy, and by NASA grants NNX08AW31G, NNX11A043G, and NNX14AQ89G and NSF grants AST-0808050 and AST-1109911. We also thank the variable star database of observations from the AAVSO International Database contributed by observers worldwide. We thank the public data observations from the Swift data archive and the Fermi Gamma-Rays Space Telescope collaboration for the public database used in this work.

## REFERENCES

- Abdo, A. A., Ackermann, M., Ajello, M., Allafort, A., Baldini, L., Ballet, J., Barbiellini, G., Baring, M. G., Bastieri, D., Bechtol, K., Bellazzini, R., Berenji, B., Blandford, R. D., Bloom, E. D., Bonamente, E., Borgland, A. W., Bouvier, A., Brandt, T. J., Bregeon, J., Brez, A., Brigida, M., Bruel, P., Buehler, R., Buson, S., Caliandro, G. A., Cameron, R. A., Cannon, A., Caraveo, P. A., Carrigan, S., Casandjian, J. M., Cavazzuti, E., Cecchi, C., Çelik, Ö., Charles, E., Chekhtman, A., Cheung, C. C., Chiang, J., Ciprini, S., Claus, R., Cohen-Tanugi, J., Conrad, J., Cutini, S., Dermer, C. D., de Palma, F., Silva, E. d. C. e., Drell, P. S., Dubois, R., Dumora, D., Favuzzi, C., Fegan, S. J., Ferrara, E. C., Focke, W. B., Fortin, P., Frailis, M., Fuhrmann, L., Fukazawa, Y., Funk, S., Fusco, P., Gargano, F., Gasparrini, D., Gehrels, N., Germani, S., Giglietto, N., Giordano, F., Giroletti, M., Glanzman, T., Godfrey, G., Grenier, I. A., Guillemot, L., Guiriec, S., Hayashida, M., Hays, E., Horan, D., Hughes, R. E., Jóhannesson, G., Johnson, A. S., Johnson, W. N., Kadler, M., Kamae, T., Katagiri, H., Kataoka, J., Knödseder, J., Kuss, M., Lande, J., Latronico, L., Lee, S. H., Lemoine-Goumard, M., Longo, F., Loparco, F., Lott, B., Lovellette, M. N., Lubrano, P., Madejski, G. M., Makeev, A., Max-Moerbeck, W., Mazziotta, M. N., McEnery, J. E., Mehault, J., Michelson, P. F., Mitthumsiri, W., Mizuno, T., Moiseev, A. A., Monte, C., Monzani, M. E., Morselli, A., Moskalenko, I. V., Murgia, S., Naumann-Godo, M., Nishino, S., Nolan, P. L., Norris, J. P., Nuss, E., Ohsugi, T., Okumura, A., Omodei, N., Orlando, E., Ormes, J. F., Paneque, D., Panetta, J. H., Parent, D., Pavlidou, V., Pearson, T. J., Pelassa, V., Pepe, M., Pesce-Rollins, M., Piron, F., Porter, T. A., Rainò, S., Rando, R., Razzano, M., Readhead, A., Reimer, A., Reimer, O., Richards, J. L., Ripken, J., Ritz, S., Roth, M., Sadrozinski, H. F. W., Sanchez, D., Sander, A., Scargle, J. D., Sgrò, C., Siskind, E. J., Smith, P. D., Spandre, G., Spinelli, P., Stawarz, L., Stevenson, M., Strickman, M. S., Sokolovsky, K. V., Suson, D. J., Takahashi, H., Takahashi, T., Tanaka, T., Thayer, J. B., Thayer, J. G., Thompson, D. J., Tibaldo, L., Torres, D. F., Tosti, G., Tramacere, A., Uchiyama, Y., Usher, T. L., Vandenbroucke, J., Vasileiou, V., Vilchez, N., Vitale,

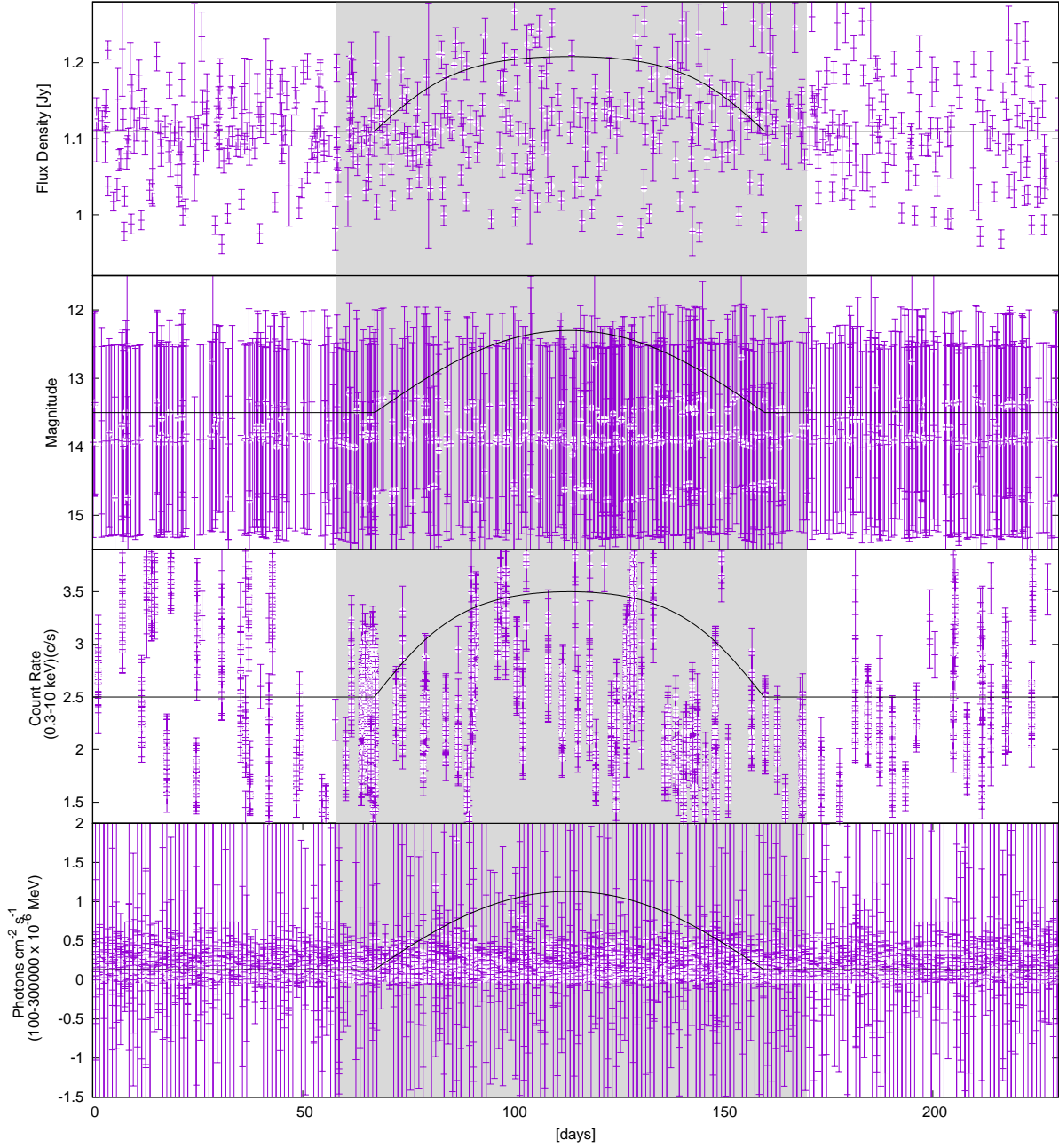


FIG. 8 From top to bottom, the figure shows 224 d folded light curves for radio, optical, x-rays and  $\gamma$ -rays. The solid curves are the best fit eclipse model described in Section III.D constructed using the results of Table VI. The shaded zone in each panel represents the duration of the eclipse.

- V., Waite, A. P., Wang, P., Wehrle, A. E., Winer, B. L., Wood, K. S., Yang, Z., Ylinen, T., Zensus, J. A., Ziegler, M., Fermi LAT Collaboration,, Aleksić, J., Antonelli, L. A., Antoranz, P., Backes, M., Barrio, J. A., Becerra González, J., Bednarek, W., Berdyugin, A., Berger, K., Bernardini, E., Biland, A., Blanch, O., Bock, R. K., Boller, A., Bonnoli, G., Bordas, P., Borla Tridon, D., Bosch-Ramon, V., Bose, D., Braun, I., Bretz, T., Camara, M., Carmona, E., Carosi, A., Colin, P., Colombo, E., Contreras, J. L., Cortina, J., Covino, S., Dazzi, F., de Angelis, A., De Cea del Pozo, E., De Lotto, B., De Maria, M., De Sabata, F., Delgado Mendez, C., Diago Ortega, A., Doert, M., Domínguez, A., Dominis Prester, D., Dorner, D., Doro, M., Elsaesser, D., Ferenc, D., Fonseca, M. V., Font, L., García López, R. J., Garczarczyk, M., Gaug, M., Giavitto, G., Godinovi, N., Hadasch, D., Herrero, A., Hildebrand, D., Höhne-Mönch, D., Hose, J., Hrupec, D., Jogler, T., Klepser, S., Krähenbühl, T., Kranich, D., Krause, J., La Barbera, A., Leonardo, E., Lindfors, E., Lombardi, S., López, M., Lorenz, E., Majumdar, P., Makariev, E., Maneva, G., Mankuzhiyil, N., Mannheim, K., Maraschi, L., Mariotti, M., Martínez, M., Mazin, D., Meucci, M., Miranda, J. M., Mirzoyan, R., Miyamoto, H., Moldón, J., Moralejo, A., Nieto, D., Nilsson, K., Orito, R., Oya, I., Paoletti, R., Paredes, J. M., Partini, S., Pasanen, M., Pauss, F., Pegna, R. G., Perez-Torres, M. A., Persic, M., Peruzzo, J., Pochon, J., Prada Moroni, P. G., Prada, F., Prandini, E., Puchades, N., Puljak, I., Reichardt, T., Reinthal, R., Rhode, W., Ribó, M., Rico, J., Rissi, M., Rügemer, S., Saggion, A., Saito, K., Saito, T. Y., Salvati, M., Sánchez-Conde, M., Satalecka, K., Scalzotto, V., Scapin, V., Schultz, C., Schweizer, T., Shayduk, M., Shore, S. N., Sierpowska-Bartosik, A., Sillanpää, A., Sitarek, J., Sobczynska, D., Spanier, F., Spiro, S., Stamerra, A., Steinke, B., Storz, J., Strah, N., Struebig, J. C., Suric, T., Takalo, L. O., Tavecchio, F., Temnikov, P., Terzić, T., Tesaro, D., Teshima, M., Vankov, H., Wagner, R. M., Weitzel, Q., Zabalza, V., Zandanel, F., Zanin, R., MAGIC Collaboration,, Acciari, V. A., Arlen, T., Aune, T., Benbow, W., Boltuch, D., Bradbury, S. M., Buckley, J. H., Bugaev, V., Cannon, A., Cesarini, A., Ciupik, L., Cui, W., Dickherber, R., Errando, M., Falcone, A., Finley, J. P., Finnegan, G., Fortson, L., Furniss, A., Galante, N., Gall, D., Gillanders, G. H., Godambe, S., Grube, J., Guenette, R., Gyuk, G., Hanna, D., Holder, J., Huang, D., Hui, C. M., Humensky, T. B., Kaaret, P., Karlsson, N., Kertzman, M., Kieda, D., Konopelko, A., Krawczynski, H., Krennrich, F., Lang, M. J., Maier, G., McArthur, S., McCann, A., McCutcheon, M., Moriarty, P., Mukherjee, R., Ong, R., Otte, A. N., Pandel, D., Perkins, J. S., Pichel, A., Pohl, M., Quinn, J., Ragan, K., Reyes, L. C., Reynolds, P. T., Roache, E., Rose, H. J., Rovero, A. C., Schroedter, M., Sembroski, G. H., Senturk, G. D., Steele, D., Swordy, S. P., Tešić, G., Theiling, M., Thibadeau, S., Varlotta, A., Vincent, S., Wakely, S. P., Ward, J. E., Weekes, T. C., Weinstein, A., Weisgarber, T., Williams, D. A., Wood, M., Zitzer, B., VERITAS Collaboration,, Villata, M., Raiteri, C. M., Aller, H. D., Aller, M. F., Arkharov, A. A., Blinov, D. A., Calciolone, P., Chen, W. P., Efimova, N. V., Kimeridze, G., Konstantinova, T. S., Kopatskaya, E. N., Koptelova, E., Kurtanidze, O. M., Kurtanidze, S. O., Lähteenmäki, A., Larionov, V. M., Larionova, E. G., Larionova, L. V., Ligustri, R., Morozova, D. A., Nikolashvili, M. G., Sigua, L. A., Troitsky, I. S., Angelakis, E., Capalbi, M., Carramiñana, A., Carrasco, L., Cassaro, P., de la Fuente, E., Gurwell, M. A., Kovalev, Y. Y., Kovalev, Y. A., Krichbaum, T. P., Krimm, H. A., Leto, P., Lister, M. L., Maccaferri, G., Moody, J. W., Mori, Y., Nestoras, I., Orlati, A., Pagani, C., Pace, C., Pearson, R., I., Perri, M., Piner, B. G., Pushkarev, A. B., Ros, E., Sadun, A. C., Sakamoto, T., Tornikoski, M., Yatsu, Y., and Zook, A., *Astrophys. J.* **727**, 129 (2011), arXiv:1011.5260 [astro-ph.HE].
- Abdo, A. A., Ackermann, M., Arimoto, M., Asano, K., Atwood, W. B., Axelsson, M., Baldini, L., Ballet, J., Band, D. L., Barbiellini, G., and et al., *Science* **323**, 1688 (2009).
- Abramowitz, M. and Stegun, I. A., *Handbook of mathematical functions with formulas, graphs, and mathematical tables*, Vol. 55 (US Government printing office, 1964).
- Ackermann, M., Ajello, M., Allafort, A., Antolini, E., Atwood, W. B., Axelsson, M., Baldini, L., Ballet, J., Barbiellini, G., Bastieri, D., Bechtol, K., Bellazzini, R., Berenji, B., Blandford, R. D., Bloom, E. D., Bonamente, E., Borgland, A. W., Bottacini, E., Bouvier, A., Bregeon, J., Brigida, M., Bruel, P., Buehler, R., Burnett, T. H., Buson, S., Caliandro, G. A., Cameron, R. A., Caraveo, P. A., Casandjian, J. M., Cavazzuti, E., Cecchi, C., Charles, E., Cheung, C. C., Chiang, J., Ciprini, S., Claus, R., Cohen-Tanugi, J., Conrad, J., Costamante, L., Cutini, S., de Angelis, A., de Palma, F., Dermer, C. D., Digel, S. W., Silva, E. d. C. e., Drell, P. S., Dubois, R., Escande, L., Favuzzi, C., Fegan, S. J., Ferrara, E. C., Finke, J., Focke, W. B., Fortin, P., Frailis, M., Fukazawa, Y., Funk, S., Fusco, P., Gargano, F., Gasparrini, D., Gehrels, N., Germani, S., Giebels, B., Giglietto, N., Giommi, P., Giordano, F., Giroletti, M., Glanzman, T., Godfrey, G., Grenier, I. A., Grove, J. E., Guiriec, S., Gustafsson, M., Hadasch, D., Hayashida, M., Hays, E., Healey, S. E., Horan, D., Hou, X., Hughes, R. E., Iafate, G., Jóhannesson, G., Johnson, A. S., Johnson, W. N., Kamae, T., Katagiri, H., Kataoka, J., Knödseder, J., Kuss, M., Lande, J., Larsson, S., Latronico, L., Longo, F., Loparco, F., Lott, B., Lovellette, M. N., Lubrano, P., Madejski, G. M., Mazziotta, M. N., McConville, W., McEnery, J. E., Michelson, P. F., Mitthumsiri, W., Mizuno, T., Moiseev, A. A., Monte, C., Monzani, M. E., Moretti, E., Morselli, A., Moskalenko, I. V., Murgia, S., Nakamori, T., Naumann-Godo, M., Nolan, P. L., Norris, J. P., Nuss, E., Ohno, M., Ohsugi, T., Okumura, A., Omodei, N., Orienti, M., Orlando, E., Ormes, J. F., Ozaki, M., Paneque, D., Parent, D., Pesce-Rollins, M., Pierbattista, M., Piranomonte, S., Piron, F., Pivato, G., Porter, T. A., Rainò, S., Rando, R., Razzano, M., Razzaque, S., Reimer, A., Reimer, O., Ritz, S., Rochester, L. S., Romani, R. W., Roth, M., Sanchez, D. A., Sbarra, C., Scargle, J. D., Schalk, T. L., Sgrò, C., Shaw, M. S., Siskind, E. J., Spandre, G., Spinelli, P., Strong, A. W., Suson, D. J., Tajima, H., Takahashi, H., Takahashi, T., Tanaka, T., Thayer, J. G., Thayer, J. B., Thompson, D. J., Tibaldo, L., Tinivella, M., Torres, D. F., Tosti, G., Troja, E., Uchiyama, Y., Vandenbroucke, J., Vasileiou, V., Vianello, G., Vitale, V., Waite, A. P., Wallace, E., Wang, P., Winer, B. L., Wood, D. L., Wood, K. S., and Zimmer, S., *Astrophys. J.* **743**, 171 (2011), arXiv:1108.1420 [astro-ph.HE].
- Aschwanden, M., *Self-organized criticality in astrophysics. The statistics of nonlinear processes in the universe* (2011).
- Aschwanden, M. J., arXiv e-prints , arXiv:1003.0122 (2010), arXiv:1003.0122 [astro-ph.SR].
- Begelman, M. C., Blandford, R. D., and Rees, M. J., *Nature (London)* **287**, 307 (1980).
- Bhatta, G., *MNRAS* **487**, 3990 (2019), arXiv:1808.06067 [astro-ph.HE].
- Blandford, R., Meier, D., and Readhead, A., *Ann. Rev. Ast. & Ast.* **57**, 467 (2019), arXiv:1812.06025 [astro-ph.HE].

- Bryce, R. and Sprague, K., *Scientific reports* **2**, 1 (2012).
- Cabrera, J. I., Coronado, Y., Benítez, E., Mendoza, S., Hiriart, D., and Sorcia, M., *MNRAS* **434**, L6 (2013), arXiv:1212.0057 [astro-ph.HE].
- Camenzind, M. and Krockenberger, M., *Astronomy and Astrophysics* **255**, 59 (1992).
- Dawson, R. I. and Fabrycky, D. C., *Astrophys. J.* **722**, 937 (2010), arXiv:1005.4050 [astro-ph.EP].
- Deeg, H. J. and Belmonte, J. A., *Handbook of exoplanets* (Springer, 2018).
- Devor, J., *Astrophys. J.* **628**, 411 (2005), arXiv:astro-ph/0504399 [astro-ph].
- Dorner, D., Adam, J., Ahnen, L. M., Baack, D., Balbo, M., Biland, A., Blank, M., Bretz, T., Bruegge, K., Bulinski, M., Buss, J., Dmytriiev, A., Einecke, S., Elsaesser, D., Hempfling, C., Herbst, T., Hildebrand, D., Kortmann, L., Linhoff, L., Mahlke, M., Mannheim, K., Mueller, A. S., Neise, D., Neronov, A., Noethe, M., Oberkirch, J., Paravac, A., Pauss, F., Rhode, W., Schleicher, B., Schulz, F., Shukla, A., Sliusar, V., Temme, F., Thaele, J., and Walter, R., *PoS ICRC2017*, 609 (2017).
- Graham, M. J., Djorgovski, S. G., Stern, D., Glikman, E., Drake, A. J., Mahabal, A. A., Donalek, C., Larson, S., and Christensen, E., *Nature* (2015).
- Gupta, A. C., Banerjee, D. P. K., Ashok, N. M., and Joshi, U. C., *Astronomy and Astrophysics* **422**, 505 (2004), arXiv:astro-ph/0405186 [astro-ph].
- Hartman, J. D. and Bakos, G. Á., *Astronomy and Computing* **17**, 1 (2016), arXiv:1605.06811 [astro-ph.IM].
- Kovacs, G., Zucker, S., and Mazeh, T., *Astronomy and Astrophysics* **391**, 369 (2002), arXiv:astro-ph/0206099 [astro-ph].
- Kurtz, D. W., *MNRAS* **213**, 773 (1985).
- Lehto, H. J. and Valtonen, M. J., *Astrophys. J.* **460**, 207 (1996).
- Lomb, N. R., *Astrophysics and Space Science* **39**, 447 (1976).
- Magallanes-Guijón, G., “Fermi-Tools Workshop: Light Curves,” (2020).
- May, R., *Nature* **26**, 457 (1976).
- Miller, H. R., Carini, M. T., and Goodrich, B. D., *Nature (London)* **337**, 627 (1989).
- Mohan, P. and Mangalam, A., *Astrophys. J.* **805**, 91 (2015), arXiv:1503.06551 [astro-ph.HE].
- Moretti, A., Campana, S., Mineo, T., Romano, P., Abbey, A. F., Angelini, L., Beardmore, A., Burkert, W., Burrows, D. N., Capalbi, M., Chincarini, G., Citterio, O., Cusumano, G., Freyberg, M. J., Giommi, P., Goad, M. R., Godet, O., Hartner, G. D., Hill, J. E., Kennea, J., La Parola, V., Mangano, V., Morris, D., Nousek, J. A., Osborne, J., Page, K., Pagani, C., Perri, M., Tagliaferri, G., Tamburelli, F., and Wells, A., in *UV, X-Ray, and Gamma-Ray Space Instrumentation for Astronomy XIV*, Society of Photo-Optical Instrumentation Engineers (SPIE) Conference Series, Vol. 5898, edited by O. H. W. Siegmund (2005) pp. 360–368.
- Narayan, R. and Bartelmann, M., “Lectures on gravitational lensing,” (1996), arXiv:astro-ph/9606001 [astro-ph].
- Padovani, P., Giommi, P., Polenta, G., Turriziani, S., D’Elia, V., and Piranomonte, S., arXiv e-prints, arXiv:1205.0647 (2012), arXiv:1205.0647 [astro-ph.HE].
- Peng, C.-K., Buldyrev, S. V., Havlin, S., Simons, M., Stanley, H. E., and Goldberger, A. L., *Phys. Rev. E* **49**, 1685 (1994).
- Press, W. H., *Comments on Astrophysics* **7**, 103 (1978).
- Quinn, J., Akerlof, C. W., Biller, S., Buckley, J., Carter-Lewis, D. A., Cawley, M. F., Catanese, M., Connaughton, V., Fegan, D. J., Finley, J. P., Gaidos, J., Hillas, A. M., Lamb, R. C., Krennrich, F., Lessard, R., McEnery, J. E., Meyer, D. I., Mohanty, G., Rodgers, A. J., Rose, H. J., Sembroski, G., Schubnell, M. S., Weekes, T. C., Wilson, C., and Zweerink, J., *ApJL* **456**, L83 (1996).
- Richards, J. L., Max-Moerbeck, W., Pavlidou, V., King, O. G., Pearson, T. J., Readhead, A. C. S., Reeves, R., Shepherd, M. C., Stevenson, M. A., Weintraub, L. C., Fuhrmann, L., Angelakis, E., Zensus, J. A., Healey, S. E., Romani, R. W., Shaw, M. S., Grainge, K., Birkinshaw, M., Lancaster, K., Worrall, D. M., Taylor, G. B., Cotter, G., and Bustos, R., *ApJS* **194**, 29 (2011a), arXiv:1011.3111 [astro-ph.CO].
- Richards, J. L., Max-Moerbeck, W., Pavlidou, V., King, O. G., Pearson, T. J., Readhead, A. C. S., Reeves, R., Shepherd, M. C., Stevenson, M. A., Weintraub, L. C., Fuhrmann, L., Angelakis, E., Zensus, J. A., Healey, S. E., Romani, R. W., Shaw, M. S., Grainge, K., Birkinshaw, M., Lancaster, K., Worrall, D. M., Taylor, G. B., Cotter, G., and Bustos, R., *ApJS* **194**, 29 (2011b), arXiv:1011.3111 [astro-ph.CO].
- Rieger, F. M. and Mannheim, K., *Astronomy and Astrophysics* **359**, 948 (2000), arXiv:astro-ph/0005478 [astro-ph].
- Roberts, D. H., Lehar, J., and Dreher, J. W., *Astronomical Journal* **93**, 968 (1987).
- Rödiger, C., Burkart, T., Elbracht, O., and Spanier, F., *Astronomy and Astrophysics* **501**, 925 (2009), arXiv:0904.4392 [astro-ph.CO].
- Scargle, J. D., *The Astrophysical Journal* **263**, 835 (1982).
- Schroeder, M. and Wiesenfeld, K., *Physics Today* **44**, 91 (1991).
- Schwarzenberg-Czerny, A., *MNRAS* **241**, 153 (1989).
- Schwarzenberg-Czerny, A., *ApJL* **460**, L107 (1996).
- Sillanpää, A., Haarala, S., Valtonen, M. J., Sundelius, B., and Byrd, G. G., *Astrophys. J.* **325**, 628 (1988).
- Smith, P. S., Montiel, E., Rightley, S., Turner, J., Schmidt, G. D., and Jannuzi, B. T., “Coordinated fermi/optical monitoring of blazars and the great 2009 september gamma-ray flare of 3c 454.3,” (2009).
- Stella, L. and Vietri, M., *ApJL* **492**, L59 (1998), arXiv:astro-ph/9709085 [astro-ph].
- Tavani, M., Cavaliere, A., Munar-Adrover, P., and Argan, A., *Astrophys. J.* **854**, 11 (2018), arXiv:1801.03335 [astro-ph.HE].
- Thieler, A. M., Rathjens, J., and Fried, R., *The RobPer-package* (2014), r package version 1.2.
- Ulrich, M.-H., Maraschi, L., and Urry, C. M., *Annual Review of Astronomy and Astrophysics* **35**, 445 (1997), <https://doi.org/10.1146/annurev.astro.35.1.445>.

VanderPlas, J. T., *ApJS* **236**, 16 (2018), arXiv:1703.09824 [astro-ph.IM].

Wagner, S. J. and Witzel, A., *Ann. Rev. Ast. & Ast.* **33**, 163 (1995).

Wang, H., Yin, C., and Xiang, F., *Astrophysics and Space Science* **362**, 99 (2017).